Journal of Magnetism and Magnetic Materials 610 (2024) 172482

Contents lists available at ScienceDirect

Journal of Magnetism and Magnetic Materials

journal homepage: www.elsevier.com/locate/jmmm

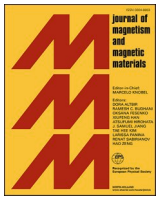

Review Article

Revisiting the concept of squareness of engineering magnetic RE-Fe-B materials hysteresis curves

E.A. Périgo [a], R.G.T. Fim [b,*], R.N. Faria [c]

[a] ABB Corporate Research Center, 1021 Main Campus Drive, Raleigh, USA
[b] Alkimat Technology, São José, Brazil
[c] Nuclear and Energy Research Institute, University of São Paulo Campus (USP-IPEN), Brazil

ARTICLE INFO

Keywords:
Magnetic films
Magnetic materials
Permanent magnets
Rectangularity
Squareness factor

ABSTRACT

The hysteresis loop shape has been a topic of interest within the area of engineering magnetic materials ranging from nano to macro scales. The literature related to its terminology, quantification propositions, significance, and relationships among proposed methods is initially revisited, clarifying potential misconceptions and illustrating its relevance in the hard-magnetic materials area. Next, relationships of the shape of the second quadrant of permanent magnets related to crystallographic alignment, microstructural features/temperature, and chemical composition/processing are discussed focusing on rare-earth-based compounds.

1. Introduction

The hysteresis curve is a typical result analyzed to evaluate the (de) magnetization behavior of (engineering) magnetic materials. Despite the possibility to directly obtain intrinsic properties (e.g. saturation polarization J_s), it commonly reports extrinsic quantities that allow the appropriate selection and implementation of engineered parts towards consumer and industrial applications.

Within this universe of extrinsic properties (including – but not limited to – remanence J_r, intrinsic coercivity H_c, and maximum energy product $(BH)_{max}$), the hysteresis curve shape is one of the relevant characteristics that both academia and industry are interested in: regarding the former, its importance is exemplified by supporting the elucidation of relationships between microstructure (e.g., (mean) grain size and its distribution, existence of secondary phases, presence of defects, and others) and reversal magnetization processes; concerning the latter, its accurate knowledge guarantees a proper application design (e.g., motors, generators, and others) that optimizes performance, reliability, and cost.

Along (at least) the last five decades, the hysteresis curve shape has been explored in studies under different contexts – as a main research topic or part of a larger effort – within a variety of magnetic materials in distinct scales including nanodots, nanowires, films, powders, and (macro) bulk parts [1–25]. The utilized terminology, shape quantification methods, and data interpretation are still ambiguous. Due to this context, the topic is addressed here to elucidate potential misconceptions and provide a brief review of the subject. Next, focusing on one of the methodologies, relationships between the quantified shape with crystallographic alignment, microstructural features/temperature, and chemical composition/processing are discussed targeting rare-earth-based compounds.

2. Terminology and quantification propositions descriptions

The hysteresis curve shape has often been quantitatively characterized by distinct means with undefined scientific/technical background. This section has been organized chronologically, reflecting a temporal development of terms and quantification propositions; further discussions on methodologies considered and/or implications are presented in the next section.

A first potential quantification of the hysteresis loop shape appears from Bozorth. Addressing materials for permanent magnets, the author focused on the second quadrant analysis of the hysteresis curve indicating the *fullness factor* γ as a function of three properties as expressed by [26]

$$\gamma = \frac{(BH)_{max}}{J_r H_c} \tag{1}$$

Smaller and Newman, about two decades later, investigated interactions effects on magnetic properties of a particulate medium [27].

* Corresponding author.
E-mail address: rafael.gitti@posgrad.ufsc.br (R.G.T. Fim).

https://doi.org/10.1016/j.jmmm.2024.172482
Received 13 May 2024; Received in revised form 26 August 2024; Accepted 27 August 2024
Available online 30 August 2024

By using iron oxide powders, the volumetric packing factor of samples was modified, and the hysteresis loop *squareness* of particle assemblies were defined – and here identified by *SS* – as

$$SS = \frac{J_r}{J_s} \tag{2}$$

In fact, Eq. (2) has also been used after Smaller and Newman to characterize the hysteresis loop shape (named as *rectangularity*) of electroless deposited iron nickel films by Djoglev et al., who indicated the relevance in achieving high *SS* values for memory elements [28].

An alternative proposition to quantity the called *squareness ratio S* of the demagnetization curve of rare earth-based permanent magnets is due to Martin et al. [29] given by

$$S \leq \frac{4\mu_0 (BH)_{max}}{J_r^2} \tag{3}$$

where μ_0 corresponds to the magnetic vacuum permeability. Another proposed approach to describe the hysteresis loop shape of permanent magnets quantitatively is reported by Yoshikawa et al. [30], here named as *squareness factor* (*SF*), and defined as

$$SF = \frac{H_k}{H_c} \tag{4}$$

where H_k corresponds to the applied magnetic field required to reduce J_r by 10 %.

A fifth methodology, proposed by Takata et al. [31], aimed the estimation of the (magnetic) quality of hard magnetic (Nd-Fe-B) melt spun powders. In this context, it has been proposed that the here called *squareness aspect*, identified by *Q*, is expressed by

$$Q = \frac{H_b}{H_c} \tag{5}$$

where H_b represents the inductive coercivity obtained from the B x H curve.

The concept of *squareness* has also been explored by Li et al. [32] indicating *SQ* dependence on J_r, J_s, and H_c with the following relation

$$SQ = \frac{\int_0^{-H_c} \frac{J}{J_s} dH}{\frac{J_r H_c}{J_s}} \tag{6}$$

More recently, the term *rectangularity* has again been used – also in the context of permanent magnet materials – when Bittner et al. defined it in [33] – and here identified by *R* – as

$$R = \frac{H_{D2}}{H_c} \tag{7}$$

where H_{D2} corresponds to the applied field at which remanence is reduced by 2 %.

3. Considerations and relationships among hysteresis curve shape quantification propositions

This section aims to analyze considerations for propositions of Eq. (1) – Eq. (7), and potential relationships between methodologies and their significances.

Starting with Eq. (1), it was (apparently) proposed in the 1950's and, therefore, before the appearance of the strongest Nd-Fe-B compounds [34,35]. Thus, such methodology apparently focused on materials classes that possess hyperbolic-like second quadrant of hysteresis loops. Theoretically, it is stated in [26] that γ ranges between 0.25 (for a linear demagnetization curve) to 1.0 (in the case of rectangular loop).

Fig. 1 depicts the second quadrant of the J x H hysteresis loop of typical Alnico, ferrite, Sm-Co, and Nd-Fe-B magnets. Although Eq. (1) might indeed be representative for Alnico, values obtained for the

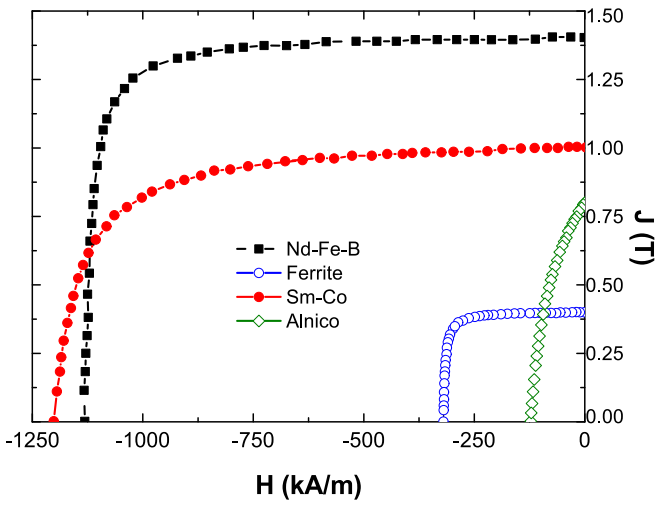

Fig. 1. Typical second quadrant of the hysteresis loop of distinct engineering hard magnetic materials.

remaining classes do not seem accurate, more specifically for those anisotropic parts that approach a rectangular shape (being closer to the unity as inferred by visual inspection). In fact, this latter observation also applies to isotropic Nd-Fe-B parts: as reported in [26], the theoretical fullness factor for $\frac{J_r}{J_s} = 0.5$ (degree of crystallographic alignment of an isotropic part – further discussed later in this section) is $\gamma = 0.34$; however, based on the data acquired experimentally in [36], one finds $\gamma = 0.10$ ($(BH)_{max} = 75$ kJm^{-3}, $J_r = 0.68$ T, and $H_c = 1.06$ MAm^{-1}), being out of scale previously indicated. Therefore, in addition to the shape of the hysteresis loop, it is possible that ranges of maximum energy product, remanence, and intrinsic coercivity (potentially of Alnico or comparable) should exist to guarantee that Eq. (1) can be satisfactorily applied. A second aspect relevant to note is that temperature will also impact Eq. (1) with magnitude being a function of distinct dependencies of $(BH)_{max}$ and H_c of each material type.

It is now appropriate to discuss the proposition from Eq. (2). Although employed in the evaluation of (soft magnetic) films and particulated media, the ratio remanence to saturation polarization has a different meaning in the area of bulk hard magnetic materials. For sintered/die upset parts, Eq. (2) is rewritten as [37]

$$\frac{J_r}{J_s} = f\langle\cos\theta\rangle(1-\beta)P \tag{8}$$

where f and $\langle\cos\theta\rangle$ represent the volumetric fraction and average crystallographic orientation of the hard-magnetic phase in the part, respectively, β indicates the sample porosity level, and P refers to the packing factor, i.e., the ratio of experimental sample density to theoretical density of the part. An important point observed in Eq. (8) refers to $\langle\cos\theta\rangle$: it is recognized (in the permanent magnets community) as a measurement of average texture – typically characterized via X-ray based techniques [38,39] –, and whose range lies within 0.5 (completely isotropic, in agreement with data provided in [26] for $\frac{J_r}{J_s}$) to 1.0 (fully anisotropic). Magnetic models (e.g. Stoner-Wohlfarth [40], with further discussion about such model for the anisotropic case available in [41]) demonstrate a clear impact of crystallographic orientation degree on the hysteresis curve shape. Thus, potential misconceptions in interpreting *SS* should be avoided (within hard magnets community): although it might indirectly provide a qualitative assessment of the hysteresis shape, the measurement itself refers to a different quantity, closely linked to the anisotropic character (crystallographic texture) of the part. In addition, Eq. (8) provides some information on the influence of (micro/macro)structure – by means of f, average crystal orientation, and porosity – on the hysteresis loop shape. At last, the temperature

dependence on Eq. (8) – for permanent magnets – might be expected to be virtually null (for temperatures at which microstructural changes do not occur) due to the relationship between J_r and J_s in *SS*.

Eq. (3) potentially uses as base the relationship between theoretical maximum energy product and remanence expressed by

$$(BH)_{max} = \frac{J_r^2}{4\mu_0} \tag{9}$$

which intrinsically adopts that the second quadrant is perfectly square/rectangular. Eq. (3) indicates that if two permanent magnets present similar values in remanence, a modification in $(BH)_{max}$ would correspond to a proportional change in *S*. This observation might not always be applicable since it is possible to manufacture permanent magnets with $S \sim 1$ and, by visual inspection, conclude that it does not fully agree with magnetic measurements as exemplified in Fig. 2.

Eq. (4) is potentially the most widely implemented in the quantitative characterization of the hysteresis loop shape of permanent magnets due to the consideration of the full second quadrant of the hysteresis loop, independently on the (an)isotropic character of the part. Although it is still not clear to the authors the reason(s) why the 10 % has been chosen for H_k determination (one historical explanation is provided in [42]), it is worth noting that it has a strong agreement (under certain conditions) with the field identified as H_{d5} described in a IEC standard [44], at least, for Nd-Fe-B magnets and which is understood as the field responsible to cause an irreversible loss of 5 % in the magnetization of a magnet. However, results can be different analyzing, for instance, bonded permanent magnets as illustrated in Fig. 3.

Eq. (5) possibly finds limited applicability in the context of permanent magnets. As *Q* uses a combination of intrinsic and inductive curves – via intrinsic and inductive coercivities, respectively –, some features of the demagnetization B x H curve must be discussed. Inductive curves with $J_r > H_c$ (commonly seen in Alnico parts and for a substantial part of ferrite offerings) present a "kink", which is more pronounced with the enhancement of squareness. On the other hand, for $H_c > J_r$ (commonly observed for Sm-Co and Nd-Fe-B parts), B x H relationship results in typically straight lines independently on its squareness (e.g., expressed by Eq. (4)). However, a perfectly squared/rectangular J x H curve with $J_r > H_c$ will result in an inductive coercivity H_b smaller than the intrinsic coercivity H_c, and therefore *Q* will not reach the maximum unity value as typically perceived for such parameter.

Eq. (6) relies in the integration of the demagnetization curve normalized by a constant that considers the maximum area of the second quadrant. There is no indication whether J_s refers to that of the hard-magnetic phase or the part under analysis. Assuming the latter and applying Eq. (6) to a permanent magnet with a perfectly square demagnetization curve, the ratio $\frac{J}{J_s}$ is a constant up to the intrinsic coercivity point. Eq. (6) then results in an absolute (unitless) value of 1.

At last, Eq. (7) seems to be a combination of the concepts presented by the squareness factor (Eq. (4)) and the IEC standard. It will be comparable to H_{d5} for a highly oriented part (since variations of *J* as a function of *H* will be minor) and present higher differences towards magnets with reduced crystallographic anisotropy due to the response of such different parts towards demagnetizing fields.

Based on the discussions provided in this section, results and correlations presented in the next subsections will utilize Eq. (4) as the backbone for assessments.

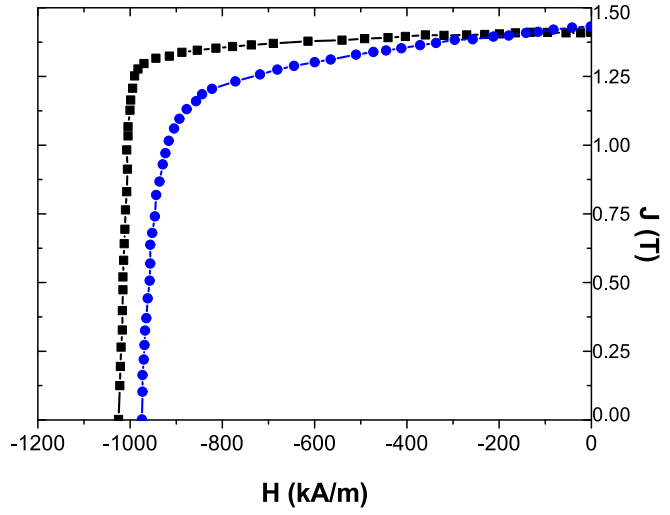

Fig. 2. Second quadrant of the hysteresis loop of magnets with composition $Nd_{13.02}Dy_{0.70}Fe_{bal}Co_{3.38}B_{6.00}Al_{1.00}Cu_{0.14}$ sintered at 1333 K (black squares) and 1353 K (blue circles). Image adapted from [43].

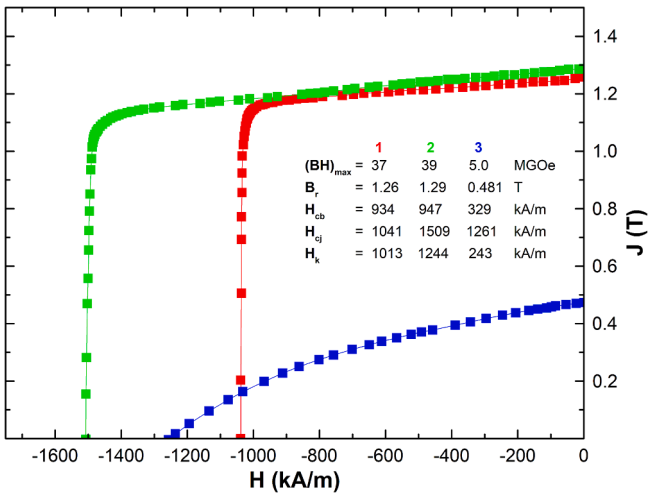

Fig. 3. Second quadrant of the hysteresis loop of Nd-Fe-B-based sintered (#1 and #2) and bonded (#3) magnets demonstrating the similarities and differences between H_{d5} and H_k. Measurements have been performed at room temperature.

4. Relationship between squareness factor and crystallographic alignment

The crystallographic alignment and squareness factor represent distinct quantities in bulk hard magnetic materials, and it is of interest to explore relationships between Eq. (4) (due to wide use in the literature) and $\langle\cos\theta\rangle$. Such relationship is depicted in Fig. 4 for sintered $Pr_{16}Fe_{76}B_8$ magnets (black triangles), where a linear variation is observed. To expand the observation scope of $\langle\cos\theta\rangle$ versus *SF* behavior, the squareness factor of sintered $Nd_{16}Fe_{78}B_6$ magnets with several crystallographic alignments was also determined from demagnetization plots reported in the literature at T=293 K [45]. In this study, texture was changed by altering the applied magnetic field and compacting pressure (crystallographic alignment was estimated using the J_r to J_s ratio). For comparison, these data are also included in Fig. 4 (red stars). The variation of the *SF* with the $\langle\cos\theta\rangle$ texture index also followed a linear relationship.

The line slope obtained from the sintered $Nd_{16}Fe_{78}B_6$ magnets is smaller than that observed for the sintered $Pr_{16}Fe_{76}B_8$ magnets, although absolute values are comparable. Furthermore, a linear relationship was observed for magnets with crystallographic alignment modified through distinct methods. In addition, it is worth noting that it is possible to modify the squareness factor of a magnet without crystallographic alignment changes. Sintered $RE_{16}Fe_{76}B_8$ magnets prepared by conventional "roller" ball milling [46] were characterized by means of magnetic properties and *SF* values. After annealing, $\langle\cos\theta\rangle$ values remained unchanged, which can be verified by means of J_r and density.

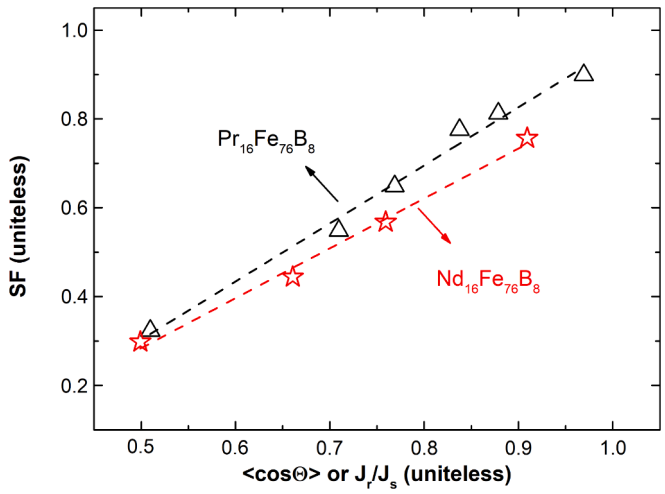

Fig. 4. *SF* variation with the ⟨cosθ⟩ texture index. Black triangles correspond to the *SF* of the sintered $Pr_{16}Fe_{76}B_8$ magnets. Red stars represent the *SF* of the $Nd_{16}Fe_{78}B_6$ sintered magnets with texture modified by changing orienting magnetic field and compaction pressure. *SF* values determined by the H_k to H_c ratio.

However, the squareness factor of both compositions was enhanced by about 30 %. A possible explanation for this behavior is the elimination of crystalline defects on the grain boundaries of the hard-magnetic phase [46].

5. Relationship of squareness factor with microstructural features and temperature

None of the proposed approaches described in Eq. (1) – Eq. (7) provides a clear link with microstructure, so that relationships with extrinsic materials features as mean grain size and its distribution, presence of phases, and others are virtually impossible to be obtained without further data. Nevertheless, it is possible to infer an imbedded microstructural linkage in Eq. (4).

In this case *SF*, as stated previously, is a measure of how square the demagnetization curve is (it is a dimensionless quantity defined by the ratio of the reverse field required to reduce the magnetization by 10 % from the remanence to the intrinsic coercivity). A squareness factor equals to one therefore corresponds to a perfectly square demagnetization loop. To reduce remanent magnetization by 10 % means that a certain amount of (non-ideal or weak) hard magnetic grains are reversing their magnetization in a reverse magnetic field smaller than the intrinsic coercivity (it is also implied that remanence is the residual or remanent magnetization of the magnetically hard grains in a closed magnetic circuit).

In a magnet composed only by perfect grains the remanent magnetization would reverse altogether in the specific field H_c. In this ideal case the hard-magnetic grains would behave similarly and there should be no reduction in the remanence until the intrinsic coercivity reverse field is reached. Non ideal magnetic grains are influenced by their inappropriate grain size, shape, distribution, sharp corners and contact with secondary phases (reversal nucleation points), precipitates and also lack of grain decoupling by a non-magnetic grain boundary phase in rare-earth magnets. All of them related to microstructural features of the permanent magnet and determinant for the value of H_k. Furthermore, it is well known that intrinsic coercivity is also affected by the same factors, but the grains that are determinant for H_c are the ones closer to perfection. Thus, simply put, the squareness factor could also be inferred as an indirect measure of the magnet microstructural behavior in relation to an ideal permanent magnet. The microstructural features of a magnet are mainly determined by the alloy composition and processing route characteristics (sintering, casting, hot pressing, etc.). A magnet with heavy rare earth addition (high H_c) but poorly processed would have an inferior squareness factor than an alloy without this addition and well processed (by decreasing H_c and increasing H_k). It is important to increase the intrinsic coercivity using addition elements and also to improve the magnet processing conditions to achieve microstructural enhanced characteristics. Nowadays, the high cost of heavy rare earth elements made much more imperative the improvement of the magnet processing routes (including recycling activities) than alloying substitution efforts. In addition, micromagnetics studies have shown that ideal grains would have a spheroid and cuboidal shapes [47].

In rare earth sintered and melt-spun magnets, *SF* has been shown to be improved with a microstructure that presents some key features, such as grain morphology, size and its distribution. A narrow grain size distribution is determinant to *SF* rather grain morphology homogeneity [5,48]. According to [49], *SF* is greatly reduced as the fraction of large grains are present in a microstructure composed of fine grains. The demagnetization mechanism in Nd-Fe-B sintered magnets is controlled by nucleation of reversal domains, preferentially taking place at the grain surface or a defect. As the grain size increases, the probability of finding a defect which acts as center for the nucleation of reversal domains increases as well. Once the reverse domain has nucleated, the magnetization of the grain switches fastly, possibly influencing the neighboring fine-grains due to magnetostatic interactions [49]. According to [50], a sum of both external magnetic field and the stray field of the reversed coarse grain increases the demagnetizing field on fine grains, contributing for a reduction on *SF* values.

In hot deformed Nd-Fe-B magnets, *SF* was significantly improved as the grain size distribution was narrowed by the suppression of regions composed of coarse and large grains, favoring the formation of fine grained regions [51]. According to [51], coarse grain regions exhibit partially oriented grains, while large grain regions are composed of randomly oriented grains, both contributing for domain reversal propagation at lower reverse fields. Increasing the fraction of fine grains, which has strong crystallographic texture and thus provides a strong pinning force of the magnetic domains, *SF* is enhanced [51].

Although temperature affect remanent magnetization and intrinsic coercivity of (RE-Fe-B) hard magnets in distinct magnitudes, the squareness factor behavior might present divergent behaviors. The squareness factor has been shown to be affected by the processing temperature (on sintering and heat treatment or annealing) and also by the temperature of measurement (or operating temperature) of N38SH-grade magnets with low oxygen content [52] as shown in Fig. 5. It was quite evident from their results that annealing the magnet at a higher temperature (853 K) led to a pronounced decrease in *SF* (from 0.94 to

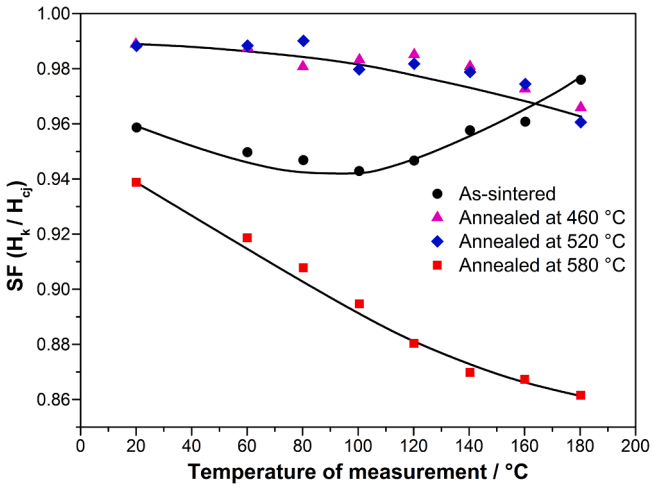

Fig. 5. Influence of the temperature of measurement on the squareness factor of Nd-Fe-B magnets annealed at distinct temperatures. Image reprinted from [52] with permission from Elsevier.

0.86) as the temperature of measurement was increased from room temperature to 453 K. Post-sintering annealing at lower temperatures (733 K and 793 K) also made the squareness factor less susceptible to the increase in the temperature of magnet operation. According to the authors, *SF* of the demagnetization curve and its temperature stability were found to decrease after annealing above the highest eutectic transition point and this has been attributed to the change of the Cu content in the Nd-rich phase under different annealing temperatures, i.e., a modification occurring at the grain boundary region [52]. This statement implied that lower annealing temperatures yield a better magnetic isolation of the magnetically hard matrix grains which is the main purpose of this rather low temperature heat treatment. Magnetic isolation of the matrix grains with a rare earth rich phase has been shown to influence considerably the squareness factor [53]. In this study the authors considered that the homogeneous distribution of intergranular phases, obtained with $(Pr,Nd)_{32.5}Fe_{62.0}Cu_{5.5}$ addition, increased rectangularity (*SF*) and maximum energy product.

Small Nd-Fe-B magnets machined to submicrometric dimensions frequently present a demagnetization curve with an irregular shape and reduced *SF*, J_r and H_c [54]. This is associated to the increase of defects on the surface of the 2:14:1 and the "peeling" of RE-rich GB phase during this operation. Oxidation and formation of soft magnetic phases are also listed as main contributions to *SF* reduction. Coating the machined surface with light or heavy REE followed by heat treatments can restore the properties to the bulk magnets via GB reconstruction and elimination of grain surface defects [52]. For comparison purposes, to find out the main reason behind the decrease in *SF* ($\frac{H_k}{H_c}$) at elevated temperatures, the effect of the anisotropy constant ratio ($\frac{K_2}{K_1}$) on *SF* for $Sr_{1-x}La_xFe_{12-x}Co_xO_{19}$ ($x = 0 - 0.4$) sintered ferrite magnets has also been studied [55]. It has been found that the value of $\frac{H_k}{H_c}$ decreases linearly as x value increases at every temperature as depicted in Fig. 6. The value of $\frac{K_2}{K_1}$ remarkably increases with increasing x value at elevated temperatures. The authors also showed that the value of $\frac{H_k}{H_c}$ linearly decreases as $\frac{K_2}{K_1}$ increases for all the magnets above room temperature and that uniaxial anisotropy has an effect on the orientation in the direction of easy magnetization and, also, that an excessive increase in $\frac{K_2}{K_1}$ is not necessarily effective to increase $\frac{H_k}{H_c}$. They concluded that the decrease in $\frac{H_k}{H_c}$ was mainly caused by the increase in $\frac{K_2}{K_1}$ at elevated temperatures.

An investigation on the coercivity enhancements of Nd–Fe–B sintered magnets by diffusing DyH_x along different axes has shown that the squareness factor is also affected by the diffusion orientation as shown in

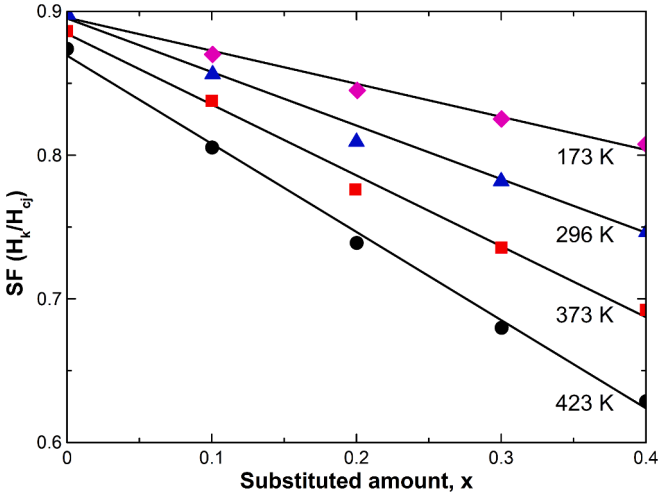

Fig. 6. Influence of the chemical composition (La content) on the squareness factor of sintered ceramic ferrite magnets. Image reprinted from [55] with permission from IEEE.

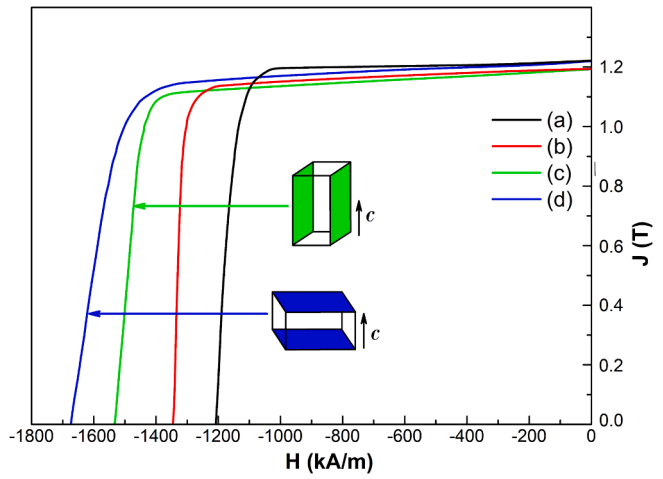

Fig. 7. Second quadrant of the hysteresis loop of Nd-Fe-B-based sintered magnets with grain boundary diffusion processes performed in distinct directions. Image reprinted from [57] with permission from IOP Publishing.

Fig. 7 [56]. These authors have shown that *SF* depends on the diffusion direction and that the *SF* value obtained by the parallel diffusion (0.876) is slightly lower than that of the perpendicular diffusion (0.93). The *SFs* for both diffused samples were lower than those of the as-sintered and annealed magnets (0.952 and 0.953). Supported by literature references, they inferred that that improved *SF* can be obtained for the magnet with a more homogenous distribution of the 2:14:1 phase grains. They concluded that since the DyH_x-treated magnets may include both Dy-diffused and Dy-free portions, composition of the local 2:14:1 phase grains differs among the whole magnet, leading to reduced *SF*. Furthermore, the *SF* of hot-deformed Nd-Fe-B permanent magnets have also been influenced by a Pr-Cu eutectic pre-diffusion process [57]. This process affected the *SF* accordingly to the amount of rare earth rich in the die-upset Nd-Fe-B magnets. Moreover, it has also been shown on the literature that addition of secondary elements on $Pr_{16}Fe_{76}B_8$ sintered commercial grade magnets ($Pr_{16}Fe_{bal}Co_{9.6}B_{5.6}Cu_{0.48}Nb_{0.06}$ and $Pr_{15.3}Fe_{bal}Co_{3.2}B_{5.8}Cu_{0.4}Nb_{0.08}$) operating at two distinct temperatures have a pronounced influence on the *SF* [12] as illustrated in Fig. 8.

6. Relationship of squareness factor with chemical composition and processing

SF has also been noticed to be influenced by the chemical composition of the magnetic alloys and therefore the final magnet, as well as content of contaminants such as oxygen and nitrogen. Nd-Fe-B melt-spun ribbons with alloying elements (i.e. Co, Zr and Ti) exhibited higher *SF* values compared to the pure Nd-Fe-B ones. This increase was attributed to the microstructural refinement effect of such alloying elements, producing a homogeneous microstructure in terms of grain size and distribution, free from soft magnetic phases [47]. Also, the "modified" ribbons were less sensitive to changes in cooling rates during their processing, allowing the obtention of optimum microstructures over a wider range of processing conditions [47]. *SF* has also been noticed to be influenced by the amount of certain light rare earth element substitution in the magnetic alloy of sintered magnets, such as Ce and La additions [58]. In the case of La and Ce substituted Nd-Fe-B melt-spun ribbons, *SF* have been reported to be reduced by both additions [59], mainly attributed to the non-uniform distribution of the La and Ce through the microstructure [59]. Nb additions up to 0.5 w.t% on Ce-containing (Nd, Ce)-Fe-B melt-spun ribbons have been shown to promote an increase of *SF* values when compared to the Nb-free ribbons, mainly due to microstructural refinement [60].

The use of alloying elements such as Nb and Zr have been shown to be necessary to increase *SF* values in Pr-Fe-B-based nanocrystalline

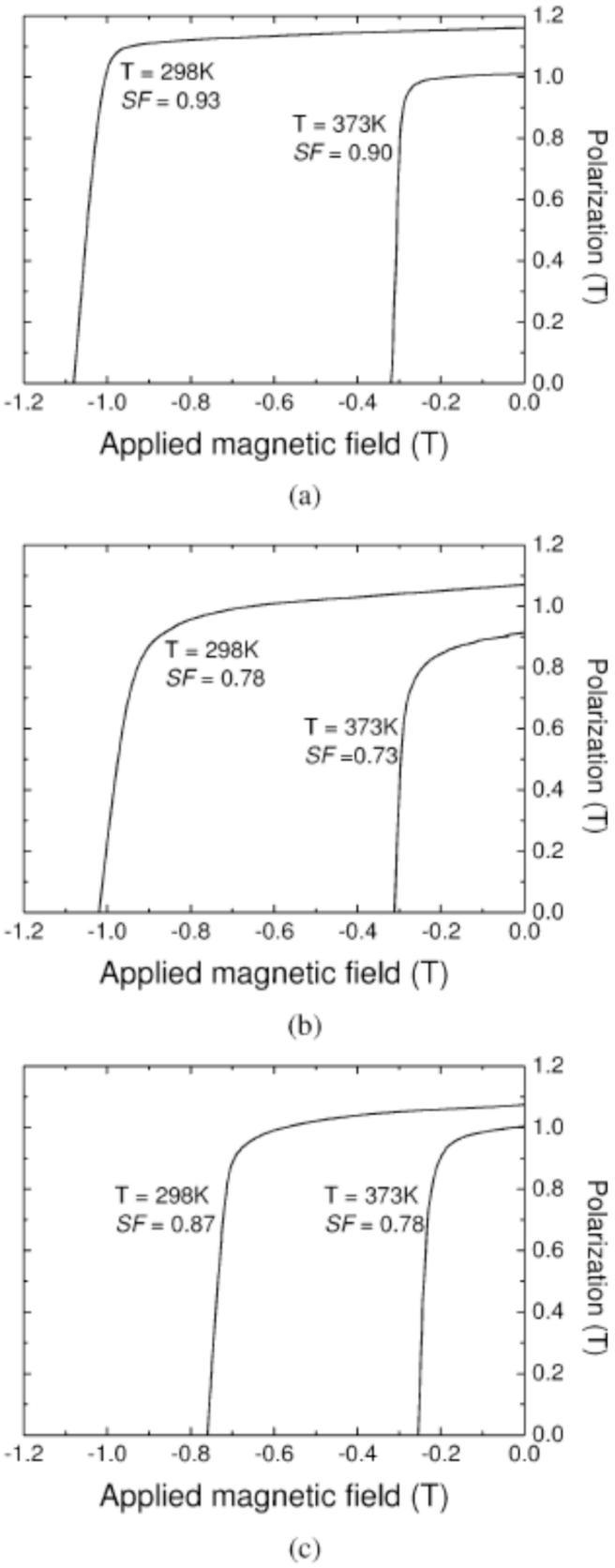

Fig. 8. Demagnetization curves of (a) $Pr_{16}Fe_{76}B_8$, (b) $Pr_{15.20}Fe_{bal}Co_{3.20}B_{5.80}Cu_{0.40}Nb_{0.08}$, and (c) $Pr_{16.60}Fe_{bal}Co_{9.60}B_{5.60}Cu_{0.80}Nb_{0.06}$ indicating variations of *SF* at distinct operating temperatures. Image reprinted from [12] with permission from IEEE.

powders obtained via HDRR [61]. Additions of 0.1 at.% maximized *SF* of the obtained powders, resulting in $H_k/H_c = 0.51$, while the Nb and Zr-free powders exhibited $H_k/H_c = 0.43$ [61]. While Nb additions allow the effective control of grain growth during the disproportion and recombination stages, Zr additions act as grain growth inhibitors during heat treatment stages, both homogenizing the microstructure in terms of grain size and size distribution [62]. Zr additions to sintered Pr-Fe-B-based magnets have also been reported to effectively increase *SF*, mainly through microstructural refinement [63,64], where sintered magnets with $H_k/H_c = 0.96$ were obtained when 0.5 at% Zr was added to the Pr-Fe-B alloy.

On multi-main-phase sintered magnets (MMP) [65], *SF* values varied between $H_k/H_c = 0.73$ and 0.93 according to post-sintering heat treatments. *SF* alterations might be linked to the optimization of the grain boundary phases and their local chemistry and the degree of inter-diffusion of La and Ce atoms from GB into the 2:14:1 grains [65]. The homogeneity of the chemical composition was attributed to be the major factor influencing *SF* values since other microstructural features (e.g., grain morphology, size, and size distribution) remained unaltered in this case, highlighting the chemical composition homogeneity importance [65]. The reduction of the Nd/Ce gradients throughout the microstructure have been demonstrated to be an effective approach to increase *SF* or sustain it at high values [66]. According to [66], increasing the Ce substitution from 9 to 18 w.t% promotes the reduction of Ce/Nd gradients from the grain surface region toward the core, allowing to sustain a high *SF*.

The oxygen content distribution also plays an important role on *SF* values of RE-based sintered magnets. It was demonstrated that a homogeneous O_2 distribution leads to an increase of the *SF* values of both Nd-Fe-B and Pr-Fe-B sintered magnets [67]. The oxides formed at the GB's act as grain growth inhibitor, refining the microstructure and therefore leading to an increase on *SF*. In the case of Pr-Fe-B sintered magnets, it was observed a progressive *SF* increase as the O_2 content increases up to 4000 ppm [67]. In the interval between 1500 – 1900 ppm O_2, H_k/H_c varied between 0.52 and 0.66, reaching $H_k/H_c = 0.8$ for 4000 ppm O_2, suggesting that an O_2 compositional gradient is rather detrimental than the oxygen presence itself [67]. In the case of Nd-Fe-B sintered magnets, *SF* values varies in a tight interval for O_2 concentrations up to 4000 ppm [67].

Recycled magnets through the *magnet-to-magnet* approach often exhibits lower *SF* values compared to the original ones, mainly associated to the oxygen increase during the reprocessing steps. The progressive recycling cycles are accompanied by a *SF* reduction which may be associated to other factors beyond heterogeneous distribution of O_2 throughout the microstructure, such as secondary phase formation, limited densification and therefore crack formation [68,69]. Additions of Nd-rich powders to the recycled magnet powder prior to sintering resulted in an increase of H_{cj} values with no further impact on *SF*. The reduction of localized defects on the grain boundaries and the partial elimination of the cracks can be the major factors for this increase. However, these additions do not improve *SF*.

In the case of rare earth based composite magnets, *SF* values can be influenced by another group of variables, specifically related to their manufacturing process, such as magnetic powder loading fraction, particle size and size distribution and porosity, as well as the other cited at previous sections. Composite magnets obtained via additive manufacturing (AM) techniques often present demagnetization loops with reduced *SF*, despite the fact the reasons for this are not discussed in depth. Isotropic RE-based composite magnets obtained via Powder-based AM (Powder Bed Fusion with Laser Beam – PBF/LB) employing different magnetic powder loading fractions and porosity levels exhibited distinct demagnetization loops [70 –72].

Despite the *SF* values were not calculated, the authors attributed this *SF* alteration to the densification level of the as-printed magnets. Porous samples clearly exhibited the tendency for demagnetization loops with lower *SF* compared to denser magnets. The reduction on *SF* values was

attributed to the rotation of loose particles within the magnet during the magnetic measurements. In the case of Sm-Fe-N composite magnets, the shape of demagnetization loop is also altered as a function of the magnetic powder loading fraction [71] or the particle size and its obtention strategy [72]. Post-printing operations for porosity reduction, such as isostatic pressing, resulted in an apparent increase of rectangularity of the demagnetization loops [73,74], supporting the negative contribution of the porosity on *SF* values. In the case of anisotropic Nd-Fe-B composite magnets [75], a similar trend is observed, where both porosity and alignment degree are variable, making difficult to precisely determine their influence on *SF* values.

The absence of *SF* evaluation is not exclusive for composite magnets obtained via Powder-based AM but can be extended to other techniques as well, such as Extrusion-based AM of strontium hexaferrites [76 –78], $Sm_2Fe_{17}N_3$ [79] and Nd-Fe-B [80].

Recently, the intrinsic demagnetization curves of permanent magnets have been derived from the electrical analogy of a 2RLC circuit as an equivalent to a magnet under demagnetization in a closed magnetic circuit [81]. This approach allows to simulate the demagnetization of a permanent magnet under different conditions and evaluate the influence of equivalent electric parameters on the demagnetization curve. Therefore, *SF* can initially be modelled according to several parameters and/or conditions, simulating different microstructural features of a permanent magnet, making possible to analyze the correlation of the features discussed along this manuscript and *SF* values from a distinct angle.

7. Conclusions

The concept of hysteresis loop squareness has been discussed exploring the development of proposed quantification methodologies, their potential inter-relations, and significance. Most propositions focused on the analysis of the second quadrant of permanent magnet-based materials (with a minor exploration towards soft magnetic compounds), indicating a common interest on the demagnetization behavior of (typical engineering) hard magnetic materials. Similarities among the proposed methods have been explored, and similarities between H_k (obtained from the squareness factor concept) and H_{d5} (from IEC standard) have been illustrated.

A general understanding of the relationship between crystallographic alignment and squareness of the hysteresis loop does exist, although divergent depending on the areas: for permanent magnets it is commonly understood that texture influences the hysteresis curve squareness, whereas in other areas there is a direct connection between both quantities. The separation in this interpretation has been discussed.

The squareness factor behavior can be affected very distinctly based on the chemical composition of the magnetic alloys (for Nd-Fe-B compounds usually related to changes in the grain boundaries), processing conditions (e.g., mean grain size, distribution of secondary phases, diffusion of alloying elements), thermal history (sintering and annealing treatments), and even operating temperatures. Therefore, the squareness factor is, in fact, a microstructural governed quantity.

In summary, the relevance of the squareness concept has been presented and aims to highlight its significance for academia and industry towards a deeper understanding among magnetization reversal processes, microstructure, and applications.

CRediT authorship contribution statement

E.A. Périgo: Writing – review & editing, Writing – original draft, Validation, Supervision, Investigation, Formal analysis, Data curation, Conceptualization. **R.G.T. Fim:** Writing – review & editing, Writing – original draft, Investigation, Formal analysis, Data curation, Conceptualization. **R.N. Faria:** .

Declaration of competing interest

The authors declare that they have no known competing financial interests or personal relationships that could have appeared to influence the work reported in this paper.

Data availability

Data will be made available on request.

Acknowledgements

EAP thanks ABB for its continuous support.

References

[1] A.S. Tehrani, M.A. Kashi, A. Ramazani, A.H. Montazer, Axially adjustable magnetic properties in arrays of multilayered Ni/Cu nanowires with variable segment sizes, Superlattices Microstruct. 95 (2016) 38–47, https://doi.org/10.1016/j.spmi.2016.04.009.
[2] W. Cui, et al., Coercivity enhancement and microstructural optimization in diffusion processed Ce-Nd-Fe-B-based films, Thin Solid Films 645 (2018) 1–4, https://doi.org/10.1016/j.tsf.2017.10.015.
[3] R. Saeki, T. Ohgai, Determination of crystal growth geometry factors and nucleation sites of electrodeposited ferromagnetic cobalt nanowire arrays, Crystals 9 (3) (2019) 142, https://doi.org/10.3390/cryst9030142.
[4] C. Luo, et al., Enhancement of magnetization damping coefficient of permalloy thin films with dilute Nd dopants, Phys. Rev. b. 89 (2014) 184412, https://doi.org/10.1103/PhysRevB.89.184412.
[5] E.A. Périgo, H. Takiishi, C.C. Motta, R.N. Faria, Microstructure and squareness factor: a quantitative correlation in (Nd, Pr)FeB sintered magnets, J. Appl. Phys. 102 (2007) 113912, https://doi.org/10.1063/1.2821756.
[6] H. Zhang, W. Jia, H. Sun, L. Guo, J. Sun, Growth mechanism and magnetic properties of Co nanowire arrays by AC electrodeposition, J. Magn. Magn. Mater. 468 (2018) 188–192, https://doi.org/10.1016/j.jmmm.2018.08.013.
[7] F. Nasirpouri, et al., Magnetic properties of electrodeposited nickel-multiwall carbon nanotube composite films, IEEE Trans. Magn. 51 (2015) 2006804, https://doi.org/10.1109/TMAG.2015.2448122.
[8] S. Wodarz, T. Hasegawa, S. Ishio, T. Homma, Structural control of ultra-fine CoPt nanodot arrays via electrodeposition process, J. Magn. Magn. Mater. 430 (2017) 52–58, https://doi.org/10.1016/j.jmmm.2017.01.061.
[9] M. Nasehnejad, G. Nabiyouni, Studying magnetic properties and surface roughness evolution of Ag-Co electrodeposited films, J. Magn. Magn. Mater. 490 (2019) 165501, https://doi.org/10.1016/j.jmmm.2019.165501.
[10] T. Chen, T. Yamashita, R. Sinclair, The effect of orientation, grain size and polymorphism on magnetic properties of sputtered Co-Re thin film media, IEEE Trans. Magn. 17 (6) (1981) 3187–3189, https://doi.org/10.1109/TMAG.1981.1061483.
[11] T. Shimatsu, H. Uwazumi, H. Muraoka, Y. Nakamura, Thermal stability in perpendicular recording media, J. Magn. Magn. Mater. 235 (2011) 273–280, https://doi.org/10.1016/S0304-8853(01)00358-4.
[12] E.A. Périgo, H. Takiishi, C.C. Motta, R.N. Faria, On the squareness factor behavior of Re-FeB (RE – Nd or Pr) magnets above room temperature, IEEE Trans. Magn. 45 (10) (2009) 4431–4434, https://doi.org/10.1109/TMAG.2009.2025190.
[13] F. Chen, T. Zhang, W. Zhang, L. Zhang, Y. Lin, Dependence of the demagnetization behavior on the direction of grain boundary diffusion in sintered Nd-Fe-B magnets, J. Magn. Magn. Mater. 465 (2018) 392–398, https://doi.org/10.1016/j.jmmm.2018.06.023.
[14] X. Xia, et al., Dissolution of two types of grain boundary phases in a hot-deformed Nd-Fe-B magnet by high-temperature annealing, Mater. Charact. 151 (2019) 64–72, https://doi.org/10.1016/j.matchar.2019.02.041.
[15] Z.H. Hu, et al., Effect of Dy addition on the magnetic and mechanical properties of sintered Nd-Fe-B magnets prepared by double-alloy powder mixed method, IEEE Trans. Magn. 51 (11) (2015), https://doi.org/10.1109/TMAG.2015.2443122.
[16] F. Xu, L. Zhang, X. Dog, Q. Liu, M. Komuro, Effect of DyF3 additions on the coercivity and grain boundary structure in sintered Nd-Fe-B magnets, Scr. Mater. 64 (2011) 1137–1140, https://doi.org/10.1016/j.scriptamat.2011.03.011.
[17] T. Song, et al., Magnetic properties improvement of hot-deformed Nd-Fe-B permanent magnets by Pr-Cu eutectic pre-diffusion process, Acta Mater. 174 (2019) 332–341, https://doi.org/10.1016/j.actamat.2019.05.065.
[18] F. Akagi, Y. Ishii, Effects of anisotropy field dispersion and grain boundary on coercivity and squareness ratio for HDDR-processed NdFeB powders, AIP Adv. 8 (2018) 056201, https://doi.org/10.1063/1.5005047.
[19] M. Zhu, et al., Influence of Ce content on the rectangularity of demagnetization curves and magnetic properties of Re-Fe-B magnets sintered by double main phase alloy method, IEEE Trans. Magn. 50 (1) (2014), https://doi.org/10.1109/TMAG.2013.2278018.
[20] H. Nishio, K.-I. Machida, K. Ozaki, More accurate hysteresis curve for large Nd-Fe-B sintered magnets employing a superconducting magnet-based vibrating sample magnetometer, IEEE Trans. Magn. 53 (4) (2017) 6000306, https://doi.org/10.1109/TMAG.2016.2641399.

[21] Y. Zhang, et al., Squareness factors of demagnetization curves for multi-main phase Nd-Ce-Fe-B magnets with different Ce contents, J. Magn. Magn. Mater. 487 (2019) 165355, https://doi.org/10.1016/j.jmmm.2019.165355.

[22] L. Le, et al., Sensitivity of coercivity and squareness factor of a Nd-Fe-B sintered magnet on post-sintering annealing temperature, J. Rare Earths. 33 (5) (2015) 507–513, https://doi.org/10.1016/S1002-0721(14)60448-8.

[23] A.M. Gabay, G.C. Hadjipanayis, J. Cui, Effect of Sb substitution on crystal structure, texture and hard magnetic properties of melt-spun MnBi alloys, J. Alloy. Compd. 792 (2019) 77–86, https://doi.org/10.1016/j.jallcom.2019.03.407.

[24] M. Srivastava, et al., Synthesis, magnetic and Mössbauer spectroscopic studies of Cr doped lithium ferrite nanoparticles, J. Alloy. Compd. 591 (2014) 174–180, https://doi.org/10.1016/j.jallcom.2013.12.180.

[25] S. Jin, T.H. Tiefel, High-remanence square loop Fe-Ni and Fe-Mn magnetic alloys, IEEE Trans. Magn. 16 (5) (1980) 1062–1064, https://doi.org/10.1109/TMAG.1980.1060677.

[26] Bozorth, R. M. (1951). **Ferromagnetism**, *D. Van Nostrand* (New York) (1951) 968p, p. 351.

[27] P. Smaller, J.J. Newman, Effect of interaction on magnetic properties of a particulate medium, IEEE Trans. Magn 6 (4) (1970) 804–808, https://doi.org/10.1109/TMAG.1970.1066987.

[28] D.J. Djoglev, I.D. Miladinova, E.V. Todorinov, I.N. Markova, On some magnetic properties of nickel iron electroless films, Thin Solid Films 14 (1972) 135–142, https://doi.org/10.1016/0040-6090(72)90375-6.

[29] D.L. Martin, H.F. Mildrum, S.R. Trout, **Squareness ratio for various rare earth permanent magnets**. *8th International Workshop on Rare Earth Permanent Magnets and Their Applications*, Dayton (USA) 1985 (1985) 269–278.

[30] N. Yoshikawa, et al., Effect of additive elements on magnetic properties and irreversible loss of hot-worked Nd-Fe-Co-B magnets, J. Appl. Phys. 69 (1991) 6049–6051, https://doi.org/10.1063/1.347766.

[31] M. Takata, et al., Nd-Fe-B melt spun powder quality estimation based on Stoner-Wohlfarth model, Commun. Phys. 14 (2004) 36–41, https://doi.org/10.15625/0868-3166/24/3S1/5234.

[32] Z. Li, et al., Variations of phase constitution and magnetic properties with Ce content in Ce-Fe-B permanent magnets, Mater. Lett. 172 (2016) 102–104, https://doi.org/10.1016/j.matlet.2016.02.149.

[33] F. Bittner, et al., Normal and abnormal grain growth in fine-grained Nd-Fe-B sintered magnets prepared from He jet milled powders, J. Magn. Magn. Mater. 426 (2017) 698–707, https://doi.org/10.1016/j.jmmm.2016.10.139.

[34] M. Sagawa, et al., New material for permanent magnets on a base of Nd and Fe (invited), J. Appl. Phys. 55 (1984) 2083–2087, https://doi.org/10.1063/1.333572.

[35] J.J. Croat, J.F. Herbst, R.W. Lee, F.E. Pinkerton, Pr-Fe and Nd-Fe-based materials: a new class of high-performance permanent magnets (invited), J. Appl. Phys. 55 (1984) 2078–2082, https://doi.org/10.1063/1.333571.

[36] E.A. Périgo, E.P. Gilbert, A. Michels, Magnetic SANS study of a sintered Nd-Fe-B magnet: estimation of defect size, Acta Mater. 87 (1) (2015) 142–149, https://doi.org/10.1016/j.actamat.2014.12.051.

[37] Z. Wang, et al., Magnetic properties improvement of die-upset Nd-Fe-B magnets by Dy-Cu press injection and subsequent heat treatment, Sci. Rep. 6 (2016) 38335, https://doi.org/10.1038/srep38335.

[38] E.A. Perigo, H. Takiishi, C.C. Motta, R.N. Faria, N.B. Lima, Determination of the crystallographic texture of sintered PrFeB magnets based on X-ray diffraction patterns, J. Magn. Magn. Mater. 320 (14) (2008) e40–e42, https://doi.org/10.1016/j.jmmm.2008.02.012.

[39] A.R.M. Castro, E. Galego, N.B. Lima, R.N. Faria, X-ray pole figure analysis of sintered PrFeB magnets, J. Magn. Magn. Mater. 278 (1–2) (2004) 39–45, https://doi.org/10.1016/j.jmmm.2003.11.371.

[40] E.C. Stoner, E.P. Wohlfarth, **A mechanism of magnetic hysteresis in heterogeneous alloys**. *Phyl*, Trans. of the Royal Soc. of London 240 (1948) 599–642, https://doi.org/10.1098/rsta.1948.0007.

[41] M.F. de Campos, F.A. Sampaio da Silva, E.A. Perigo, J.A. de Castro, Stoner-Wohlfarth model for the anisotropic case, J. Magn. Magn. Mater 345 (2013) 147–152, https://doi.org/10.1016/j.jmmm.2013.06.028.

[42] Arnold Magnetic Technologies, Technical Notes, **Hk: A Magnetic Figure of Merit**, https://www.arnoldmagnetics.com/wp-content/uploads/2017/10/Hk-A-Key-Magnetic-Figure-of-Merit-TN_0901_rev_160212.pdf, 2016 (accessed 9 May 2024).

[43] K. Yamamoto, T. Nishigouri, M. Shimao, M. Kusunoki, T. Minowa, **Effect of Zr on the low oxygen NdFeB sintered magnets**, *17th International Workshop on Rare Earth Permanent Magnets and their Applications*, Delaware 2002 (2002) 648–655.

[44] International Electrotechnical Commission. (2015). Magnetic materials Part 8.1: Specification for individual materials – magnetically hard materials (IEC standard 60404-8-1, edition 3.0).

[45] A. Handstein, K.-H. Müller, D. Eckert, P. Nothnagel, The dip in the magnetization curves of sintered Nd-Fe-B magnets with different degrees of texture, J. Magn. Magn. Mater. 101 (1991) 382–384, https://doi.org/10.1016/0304-8853(91)90787-B.

[46] Faria, R. N., Williams, A. J., Abell, J. S., & Harris, I. R. (1996). **Magnetic properties of Pr-Fe-B sintered magnets produced from hydride powder and from partially and totally desorbed hydride powder**. *Proceedings of the 14th International Workshop on Rare Earth Permanent Magnets and Their Applications*, edited by F. P. Missel (1996) 570-579.

[47] M. Yi, O. Gutfleisch, Micromagnetic simulations on the grain shape effect in Nd-Fe-B magnets, J. Appl. Phys. 120 (2016) 033903, https://doi.org/10.1063/1.4958697.

[48] D.J. Branagan, M.J. Kramer, Y.L. Tang, R.W. McCallum, Maximizing loop squareness by minimizing gradients in the microstructure, J. Appl. Phys. 85 (1999) 5923–5925.

[49] R. Ramesh, G. Thomas, B.M. Ma, Magnetization reversal in nucleation controlled magnets. II. effect of grain size and size distribution on intrinsic coercivity of Fe-Nd-B magnets, J. Appl. Phys 64 (11) (1988) 6416–6423, https://doi.org/10.1063/1.342055.

[50] F. Bittner, T.G. Woodcock, L. Schultz, C. Schwöbel, O. Gutfleisch, G.A. Zickler, J. Fidler, K. Üstüner, M. Katter, Normal and abnormal grain growth in fine-grained Nd-Fe-B sintered magnets prepared from He jet milled powders, J. Magn. Magn. Mater 426 (2017) 698–707, https://doi.org/10.1016/j.jmmm.2016.10.139.

[51] Y. Li, X. Xu, M. Yue, T. Ma, W. Liu, Correlation between microstructural heterogeneity and energy product in hot deformed Nd-Fe-B magnets, J. Magn. Magn. Mater. 508 (2020) 166847, https://doi.org/10.1016/j.jmmm.2020.166847.

[52] L. Liang, M. Wu, L. Liu, C. Ma, J. Wang, J. Zhang, L. Zhang, Sensitivity of coercivity and squareness factor of a Nd-Fe-B sintered magnet on post-sintering annealing temperature, J. Rare Earths. 33 (5) (2015) 507–513, https://doi.org/10.1016/s1002-0721(14)60448-8.

[53] M. Yan, J. Jin, T. Ma, Grain boundary restructuring and La/Ce/Y application in Nd–Fe–B magnets, Chin. Phys. b. 28 (7) (2019) 077507, https://doi.org/10.1088/1674-1056/28/7/077507.

[54] S. Hirosawa, K. Tokuhara, M. Sagawa, Coercivity of surface grains of Nd-Fe-B sintered magnet, Jpn. J. Appl. Phys. 26 (8A) (1987), https://doi.org/10.1143/jjap.26.l1359.

[55] H. Nishio, **Effect of anisotropy constants on squareness ratio in Sr–La–Co high-performance sintered ferrite magnets at elevated temperatures** *IEEE Trans*, Magn. 51 (5) (2015) 2100204, https://doi.org/10.1109/TMAG.2015.2406007.

[56] T. Ma, X. Wang, X. Liu, C. Wu, M. Yan, Coercivity enhancements of Nd–Fe–B sintered magnets by diffusing DyHx along different axes, J. Phys. d: Appl. Phys. 48 (21) (2015) 215001, https://doi.org/10.1088/0022-3727/48/21/215001.

[57] T. Song, X. Tang, W. Yin, J. Ju, Z. Wang, Q. Liu, Y. Tang, R. Chen, A. Yan, Magnetic properties improvement of hot-deformed Nd–Fe–B permanent magnets by Pr–Cu eutectic pre-diffusion process, Acta Mater. 174 (2019) 332–341, https://doi.org/10.1016/j.actamat.2019.05.065.

[58] Y. Zhang, T. Ma, J. Jin, J. Li, C. Wu, B. Shen, M. Yan, Effects of REFe2 on microstructure and magnetic properties of Nd-Ce-Fe-B sintered magnets, Acta Mater. 128 (2017) 22–30, https://doi.org/10.1016/j.actamat.2017.02.002.

[59] M. Hussain, L.Z. Zhao, R. Akram, Z. Ahmad, Z.Y. Zhang, A. Gulzar, X.C. Zhong, Z. W. Liu, Magnetic properties and exchange interaction of rapidly quenched La or Ce substituted nanocrystalline NdFeB alloys with various compositions, J. Magn. Magn. Mater. 468 (2018) 141–147, https://doi.org/10.1016/j.jmmm.2018.07.089.

[60] Q. Quan, L. Zhang, Q. Jiang, W. Lei, Q. Zeng, X. Hu, L. Wang, X. Yu, J. Du, G. Fu, R. Liu, M. Zhong, Z. Zhong, Effect of Nb doping on the microstructure and magnetic properties of Nd-Ce-Fe-B alloy, J. Magn. Magn. Mater. 442 (2017) 377–382, https://doi.org/10.1016/j.jmmm.2017.07.017.

[61] R.N. Faria, D.N. Brown, I.R. Harris, The influence of alloying additions and process parameters on the magnetic properties of PrFeB-based bonded magnets, J. Alloy. Compd. 296 (1–2) (2000) 219–222, https://doi.org/10.1016/S0925-8388(99)00535-6.

[62] N. Cannesan, D.N. Brown, A.J. Williams, I.R. Harris, The production and characterisation of highly anisotropic PrFeCoB-type HDDR powders, J. Magn. Magn. Mater. 233 (3) (2001) 209–218, https://doi.org/10.1016/S0304-8853(01)00212-8.

[63] R.N. Faria, The influence of zirconium addition and process parameters on the magnetic properties of Pr-Fe-B sintered magnets, J. Magn. Magn. Mater. 238 (1) (2002) 56–64, https://doi.org/10.1016/S0304-8853(01)00701-6.

[64] R.N. Faria, H. Takiishi, L.F.C.P. Lima, I. Costa, Praseodymium-based HD-sintered magnets produced using a mixture of cast alloys, J. Magn. Magn. Mater. 237 (3) (2001) 261–266, https://doi.org/10.1016/S0304-8853(01)00692-8.

[65] H. Chen, W. Liu, Y. Yin, Z. Li, Z. Wang, Y. Li, M. Yue, Z. Pang, X. Yu, C. Yu, Achievement of high performance in multi-main-phase (Pr, Nd, MM)-Fe-B sintered magnets by regulating microstructure, Intermetallics 124 (2020) 106870, https://doi.org/10.1016/j.intermet.2020.106870.

[66] Y. Zhang, T. Ma, M. Yan, J. Jin, X. Liu, F. Xu, X. Miao, C. Liu, Squareness factors of demagnetization curves for multi-main-phase Nd-Ce-Fe-B magnets with different Ce contents, J. Magn. Magn. Mater. 487 (2019) 165355, https://doi.org/10.1016/j.jmmm.2019.165355.

[67] M.R. Corfield, I.R. Harris, A.J. Williams, Influence of oxygen content on grain growth in Pr–Fe–B/Nd–Fe–B sintered magnets, J. Alloy. Compd. 463 (1–2) (2008) 180–188, https://doi.org/10.1016/j.jallcom.2007.09.057.

[68] M. Schönfeldt, U. Rohrmann, P. Schreyer, M. Hasan, K. Opelt, J. Gassmann, A. Weidenkaff, O. Gutfleisch, Magnetic and structural properties of multiple recycled and sustainable sintered Nd-Fe-B magnets, J. Alloy. Compd. 939 (2023) 168709, https://doi.org/10.1016/j.jallcom.2023.168709.

[69] M. Zakotnik, I.R. Harris, A.J. Williams, Multiple recycling of NdFeB-type sintered magnets, J. Alloy. Compd. 469 (1–2) (2009) 314–321, https://doi.org/10.1016/j.jallcom.2008.01.114.

[70] R.G.T. Fim, A.A. Mascheroni, L.F. Antunes, J.B.E. Engerroff, C.H. Ahrens, P.A. P. Wendhausen, Increasing packing density of Additively Manufactured Nd-Fe-B bonded magnets, Addit. Manuf. 35 (2020) 101353, https://doi.org/10.1016/j.addma.2020.101353.

[71] M. Röhrig, R.G.T. Fim, R.N. Faria, C.C. Plá Cid, C.H. Ahrens, P. Wendhausen, **Laser powder bed fusion of Sm-Fe-N bonded magnets employing flake powders.**, *3D Print*, Addit. Manuf. 11 (1) (2024) 171–178, https://doi.org/10.1089/3dp.2021.0228.

[72] M. Röhrig, R.G.T. Fim, L.T. Quispe, F.J.G. Landgraf, C.H. Ahrens, C.C. Plá Cid, P.A. P. Wendhausen, On the feasibility of using Sm2Fe17Nx powders obtained via

HDDR process for laser powder bed fusion of bonded permanent magnets, J. Magn. Magn. Mater. 565 (2023) 170273, https://doi.org/10.1016/j.jmmm.2022.170273.
[73] A.B. Baldissera, P. Pavez, P.A.P. Wendhausen, C.H. Ahrens, J.M. Mascheroni, Additive Manufacturing of Bonded Nd–Fe–B—Effect of Process Parameters on Magnetic Properties, IEEE Trans. Magn. 53 (11) (2017) 1–4, https://doi.org/10.1109/TMAG.2017.2715722.
[74] J.A.B. Engerroff, A.B. Baldissera, M.D. Magalhães, P.H. Lamarão, P.A. P. Wendhausen, C.H. Ahrens, J.M. Mascheroni, Additive manufacturing of Sm-Fe-N magnets, J. Rare Earths. 37 (10) (2019) 1078–1082, https://doi.org/10.1016/j.jre.2019.04.012.
[75] K. Schäfer, R.G.T. Fim, F. Maccari, T. Braun, S. Riegg, K.P. Skokov, D. Koch, E. Bruder, I. Radulov, C.H. Ahrens, P.A.P. Wendhausen, O. Gutfleisch, Laser powder bed fusion of anisotropic Nd-Fe-B bonded magnets utilizing an in-situ mechanical alignment approach, J. Magn. Magn. Mater 583 (2023) 171064, https://doi.org/10.1016/j.jmmm.2023.171064.
[76] F. Yang, X. Zhang, Z. Guo, S. Ye, Y. Sui, A.A. Volinsky, 3D printing of NdFeB bonded magnets with SrFe12O19 addition, J. Alloy. Compd. 779 (2019) 900–907, https://doi.org/10.1016/j.jallcom.2018.11.335.
[77] C. Huber, C. Abert, F. Bruckner, M. Groenefeld, S. Schuschnigg, I. Teliban, C. Vogler, G. Wautischer, R. Windl, D. Suess, 3D printing of polymer-bonded rare-earth magnets with a variable magnetic compound fraction for a predefined stray field, Sci. Rep. 7 (1) (2017) 9419, https://doi.org/10.1038/s41598-017-09864-0.
[78] M. Suppan, C. Huber, K. Mathauer, C. Abert, F. Brucker, J. Gonzalez-Gutierrez, S. Schuschnigg, M. Groenefeld, I. Teliban, S. Kobe, B. Saje, D. Suess, In-situ alignment of 3D printed anisotropic hard magnets, Sci. Rep. 12 (1) (2022) 17590, https://doi.org/10.1038/s41598-022-20669-8.
[79] K. Gandha, M.P. Paranthaman, B.C. Sales, H. Wang, A. Dalagan, T.N. Lamichhane, D.S. Parker, I.C. Nlebedim, 3D printing of anisotropic Sm–Fe–N nylon bonded permanent magnets, Eng. Rep. 3 (12) (2021) e12478.
[80] K. Gandha, I.C. Nlebedim, V. Kunc, E. Lara-Curzio, R. Fredette, M. Paranthaman, Additive manufacturing of highly dense anisotropic Nd–Fe–B bonded magnets, Scr. Mater. 183 (2020) 91–95, https://doi.org/10.1016/j.scriptamat.2020.03.012.
[81] A.P.R. Fernandez, E.A. Perigo, R.N. de Faria Junior, Modelling and simulation of electrical analogous for permanent magnet materials, Phys. Scr. 98 (11) (2023) 115025, https://doi.org/10.1088/1402-4896/ad0079.